# RETRIEVAL OF SOURCE PARAMETERS OF AN EVENT OF THE 2000 WEST BOHEMIA EARTHQUAKE SWARM ASSUMING AN ANISOTROPIC CRUST

D. RÖSSLER[1], F. KRÜGER[1], I. PŠENČÍK[2], G. RÜMPKER[3]

1 Institut für Geowissenschaften, Universität Potsdam, Karl-Liebknecht-Str. 24, D-14476 Potsdam-Golm, Germany (diroess@uni-potsdam.de, kruegerf@uni-potsdam.de)

2 Geophysical Institute, Acad. Sci. Czech Republic, Boční II/1401, 141 31 Prague 4, Czech Republic (ivan@ig.cas.cz)

3 Institut für Geowissenschaften, Universität Frankfurt/Main, Feldbergstr. 47, D-60323 Frankfurt/Main, Germany (rumpker@geophysik.uni-frankfurt.de)

*Received: March 29, 2006; Revised: February 4, 2007; Accepted: February 7, 2007*

## ABSTRACT

*We propose an inversion scheme for retrieval of characteristics of seismic point sources, which in contrast to common practice, takes into account anisotropy. If anisotropy is neglected during inversion, the moment tensors retrieved from seismic waves generated by sources situated in anisotropic media may be biased. Instead of the moment tensor, the geometry of the source is retrieved directly in our inversion; if necessary, the moment tensor can be then determined from the source geometry aposteriori. The source geometry is defined by the orientation of the slip vector and the fault normal as well as the strength of the event given by the size of the slip and the area of the fault. This approach allows direct interpretation of the source geometry in terms of shear and tensile faulting. It also makes possible to identify volumetric source changes that occur during rupturing.*

*We apply the described algorithm to one event of the 2000 West Bohemia earthquake swarm episode. For inversion we use information of the direct P waves. The structure is approximated by three different models determined from travel-time observations. The models are inhomogeneous isotropic, inhomogeneous anisotropic, and homogeneous anisotropic. For these models we obtain seismic moments* $M_T = 3.2 - 3.8 \times 10^{14}$ *Nm and left-lateral near-vertical oblique normal faulting on a N-S trending rupture surface. The orientation of the rupture surface is consistent with fault-plane solutions of earlier studies and with the spatial distribution of other events during this swarm. The studied event seems to be accompanied by a small amount of crack opening. The amount of crack opening is slightly reduced when the inhomogeneous anisotropic model is assumed, but it persists. These results and additional independent observations seem to indicate that tensile faulting occurs as a result of high fluid pressure.*

Key words: seismic source, tensile faulting, seismic anisotropy, West Bohemia

## 1. INTRODUCTION

Seismic moment tensors are retrieved from waveforms to describe the orientation and the strength of point sources. They are routinely determined under the assumption that the medium around the source and along the ray-path is isotropic. Anisotropic material properties are usually neglected during the inversion. However, the radiation pattern of seismic sources may be affected by anisotropy (see e.g. *Kawasaki and Tanimoto, 1981*; *Gajewski, 1993*; *Pšenčík and Teles, 1996*; *Rössler et al., 2004*). This may lead to the occurrence of apparent non-double-couple moment-tensor components (see e.g. *Rössler et al., 2004*; *Vavryčuk, 2005*; *Rössler et al., 2007*). On the contrary, by neglecting anisotropy, true volumetric components may become invisible in moment tensors. The effect of anisotropy on moment tensors depends on the strength of anisotropy and on the orientation of the anisotropic elastic tensor with respect to the geometry of the source.

Moment tensors can be decomposed into the double-couple component (DC) quantifying the amount of shear faulting, the compensated-linear-vector-dipole component (CLVD), and the isotropic component (ISO) providing information on possible volumetric source changes that occur during faulting (*Jost and Herrmann, 1989*; *Aki and Richards, 2002*). Faulting events that comprise volumetric source changes are also called tensile earthquakes. Non-double-couple components of moment tensors can be caused by tensile faulting, e.g., due to fluid interaction, processes involving net forces, complex fault geometries, structural mismodelling, and anisotropy (see *Julian et al., 1998*; *Miller et al., 1998*, for an overview). They are often ignored because of their sensitivity to the use of inappropriate Green's functions or insufficient ray coverage (*Sipkin, 1986a*; *Kuge, 1994*; *Henry et al., 2002*).

Non-double-couple components have been frequently observed and also interpreted in terms of tensile faulting (see e.g. *Sykes, 1967*; *Solomon and Julian, 1974*; *Sipkin, 1986b*; *Kanamori et al., 1993*; *Julian et al., 1997*; *Dreger et al., 2000*; *Dahm et al., 2000*; *Vavryčuk, 2001,2002*; *Foulger et al., 2004*). Observed volumetric source components may be indicative of the role of fluids during rupturing, and mineral phase changes at greater depth or may image existing pathways enabling fluid migration in carbonhydrate production fields. In these cases accurate and indisputable determination of tensile components is of primary interest. Without knowledge of anisotropy at the source, the reliability of interpretations of the moment tensor in terms of volumetric source changes must be questioned (*Vavryčuk, 2005*; *Rössler et al., 2007*). We therefore propose an inversion scheme for dislocation point sources taking into account inhomogeneity and anisotropy of the medium. For such sources, we directly invert observed seismograms for the direction of slip and fault normal. Working with these quantities provides a direct image of the dislocation instead of the forces acting at the source. The direction of slip and fault normal can be used to determine the elements of the moment tensor, which is usually sought in the source studies.

We apply the inversion algorithm to one event that occurred during the earthquake swarm in West Bohemia (Central Europe) in 2000. Direct P waves are used during inversions.

Roman lower-case indices $i$, $j$, $k$, $p$, $q$ attain values 1, 2, 3, lower-case Greek indices $\alpha$ and $\beta$ attain values $1, 2, \ldots, 6$. Einstein summation convention is used for repeated indices.

## 2. FORWARD MODELLING IN INHOMOGENEOUS ANISOTROPIC MEDIA

For seismic body waves travelling in anisotropic media the *i*-th component $u_i$ of the far-field complex-valued displacement at a location $\boldsymbol{x}$ due to a moment point source at $\boldsymbol{x}_0$ is given in the ray-theoretical high-frequency approximation (*Pšenčík and Teles, 1996*):

$$u_i(\boldsymbol{x},t) = g_i(\boldsymbol{x})\left[\frac{\rho(\boldsymbol{x}_0)c(\boldsymbol{x}_0)}{\rho(\boldsymbol{x})c(\boldsymbol{x})}\right]^{1/2} \frac{D\, f^{(A)}\left(t-\tau(\boldsymbol{x})\right)}{\left|\Omega_M(\boldsymbol{x})\right|^{1/2}} \exp\left[\mathrm{i}\frac{\pi}{2}k_s - \mathrm{i}\frac{\pi}{2}k(\boldsymbol{x}_0,\boldsymbol{x})\right]. \quad (1)$$

Actual seismograms are given by the real part of the displacement $\mathrm{Re}\left(u_i(\boldsymbol{x},t)\right)$. Note that the approximation (1) is applicable to P waves and well separated S waves. Eq.(1) suffers from the limitations of the ray theory, see, e.g., *Červený (2001)*. We should thus expect its lower accuracy in caustic regions of both waves and in singular directions of S waves.

The quantity *D* in Eq.(l) denotes the directivity given by

$$D(\boldsymbol{x}_0,\theta,\varphi) = \frac{g_j(\boldsymbol{x}_0)M_{jk}\,p_k(\boldsymbol{x}_0)}{4\pi\rho(\boldsymbol{x}_0)c(\boldsymbol{x}_0)}. \quad (2)$$

The directivity (2) represents a spreading-free amplitude at the source. It should not be confused with the directional dependence of amplitudes due to source finiteness. It depends on the moment tensor $M_{jk}$, the polarisation and the slowness vectors, $g_j$ and $p_k$, respectively, as well as on the phase velocity $c$ and the density $\rho$ at the source. The slowness vector $p_k$ at the source is specified by the take-off angles $\theta$ and $\varphi$.

In Eq.(1), $\Omega_M$ is related to the relative geometrical spreading $\left|\Omega_M\right|$, $g_i(\boldsymbol{x})$ is the polarisation vector at $\boldsymbol{x}$, and $f^{(A)}$ is the analytical signal corresponding to the source time function. The integer quantities *k* and $k_s$ are the indices of the trajectory and of the source, respectively (see *Pšenčík and Teles, 1996*, for a detailed description). Note that we are referring to a right-handed coordinate system: $N, E, Z \rightarrow x_1, x_2, x_3$, but observed seismograms are recorded in the left-handed coordinate system: *N*, *E*, *Z* with *Z* pointing positive up.

For dislocation point sources, the source geometry is described by the unit slip vector $\boldsymbol{s}$, the unit normal $\boldsymbol{n}$ to the fault plane, and the potency which is the product of the fault area $A_0$ with the magnitude *S* of the slip in the direction of $\boldsymbol{s}$ (*Aki and Richards, 2002*). Elastic moduli $c_{jkpq}$, that describe medium properties in the vicinity of the source, and source geometry define the moment tensor $M_{jk}$ (*Aki and Richards, 2002*):

$$M_{jk} = c_{jkpq}s_p n_q S A_0. \quad (3)$$

From Eq.(3), we can see that different properties of the moment tensor arise from sources in isotropic and anisotropic media. For example, shear faulting in anisotropic media may produce moment tensors which have the character of tensile earthquakes in isotropic

media, i.e. shear faulting accompanied by some amount of opening or closing of the fault during rupturing (see e.g. *Rössler et al., 2004*; *Vavryčuk, 2005*).

We can also express the moment tensor in Eq.(3) in terms of the source tensor $D_{pq}$:

$$M_{jk} = c_{jkpq} D_{pq}\,, \tag{4}$$

where $D_{pq}$ is formed by the dyadic product of the slip and the fault normal

$$D_{pq} = \frac{1}{2} SA_0 \begin{pmatrix} 2s_1n_1 & s_1n_2 + s_2n_1 & s_1n_3 + s_3n_1 \\ s_1n_2 + s_2n_1 & 2s_2n_2 & s_2n_3 + s_3n_2 \\ s_1n_3 + s_3n_1 & s_2n_3 + s_3n_2 & 2s_3n_3 \end{pmatrix}. \tag{5}$$

Elements of the source tensor $D_{pq}$ make up 6 elementary sources $\sigma_\alpha$, which are components of the source vector $\boldsymbol{\sigma}$

$$\boldsymbol{\sigma}^T = SA_0 \left( s_1n_1,\ s_2n_2,\ s_3n_3,\ s_2n_3 + s_3n_2,\ s_1n_3 + s_3n_1,\ s_1n_2 + s_2n_1 \right). \tag{6}$$

Inserting Eqs.(2), (3), and (6) into Eq.(1), we can express the seismograms in terms of the elementary sources $\sigma_\alpha$

$$\mathrm{Re}\left( u_i\left(\boldsymbol{x},t\right)\right) = Y_{i\alpha}\,\mathrm{Re}\left( f^{(A)}\left(t-\tau\left(\boldsymbol{x}\right)\right)\exp\left[ \mathrm{i}\frac{\pi}{2}k_s - \mathrm{i}\frac{\pi}{2}k\left(\boldsymbol{x}_0,\boldsymbol{x}\right)\right]\right)\sigma_\alpha\,. \tag{7}$$

For $Y_{i\alpha}$ see Appendix A. The left-hand side of Eq.(7) is determined from observed seismograms. All quantities appearing on the right-hand side of Eq.(7), except $\sigma_\alpha$, are obtained by forward modelling of waves in inhomogeneous anisotropic media using the software package ANRAY (*Pšenčík, 1998*).

## 3. INVERSE PROBLEM

The system of equations (7) corresponding to observations at different receivers can be solved for the components of the source vector $\boldsymbol{\sigma}$. Hereby, we use a linear least square approach (see *Menke, 1989*) to minimise the squared misfit $\boldsymbol{\varepsilon}^T\boldsymbol{\varepsilon}$. Symbol $\boldsymbol{\varepsilon}$ denotes the misfit vector of both sides of Eq.(7) in the form

$$\boldsymbol{\varepsilon} = \boldsymbol{d} - \mathbf{A}\boldsymbol{\sigma}\,, \tag{8}$$

where $\boldsymbol{d}$ is the data vector composed of all samples of all seismograms used for inversion (left-hand side of Eq.(7)) and $\mathbf{A}\boldsymbol{\sigma}$ represents the right-hand side of Eq.(7). The residual $R$ is obtained as a relative measure of the misfit by normalisation of the squared misfit to the square of the length of the data vector

$$R = \frac{\boldsymbol{\varepsilon}^T\boldsymbol{\varepsilon}}{\boldsymbol{d}^T\boldsymbol{d}}\,. \tag{9}$$

In this way, residuals are less dependent of observed amplitudes, and residuals for events with different strength are comparable. $R$ is used to evaluate the solutions of inversions. Small values of $R$ indicate good data fit.

We seek the source vector $\boldsymbol{\sigma}$ by inversion of seismograms of observed direct P waves. The inversion is carried out in the time domain. Misalignment of observed and synthetic seismograms often occurs due to inaccurate phase picking. For time-domain inversion this may cause spurious non-shear components in retrieved source geometries. Phase alignment is therefore carried out in 3 steps prior to the inversion:

1 Observed phases are manually picked. A time window for inversion is defined.
2 Within the time window observed phases are manually aligned with the computed synthetic seismograms.
3 Automatic cross-correlation is applied to align data and synthetics. A threshold based on the correlation coefficient may be used to define if data are to be included in inversion.

The efficiency of the algorithm is demonstrated by inversion of synthetic seismograms in *Rössler et al. (2005)*.

## 4. INTERPRETATION OF INVERSION RESULTS

A singular value decomposition of $D_{pq}$ in Eq.(5) yields the eigenvalues $\nu_1 = SA_0/2(s_i n_i + 1)$, $\nu_2 = 0$, $\nu_3 = SA_0/2(s_i n_i - 1)$ (compare *Vavryčuk, 2005*). The corresponding (normalised) eigenvectors are $\boldsymbol{e}_1 = (\boldsymbol{s}+\boldsymbol{n})/|\boldsymbol{s}+\boldsymbol{n}|$, $\boldsymbol{e}_2 = (\boldsymbol{s}\times\boldsymbol{n})/|\boldsymbol{s}\times\boldsymbol{n}|$, and $\boldsymbol{e}_3 = (\boldsymbol{s}-\boldsymbol{n})/|\boldsymbol{s}-\boldsymbol{n}|$, where $\times$ denotes the vectorial product. In the following we calculate the slip inclination $\delta$, i.e. the angle between the direction of the slip and the fault normal, $\cos(\delta) = |s_i n_i|$, from the eigenvalues of $D_{pq}$ formed from the retrieved elements $\sigma_\alpha$

$$\cos(\delta) = \frac{\nu_1 + \nu_3}{\nu_1 - \nu_3}. \tag{10}$$

For pure shear faulting, $\delta = 90°$, but $\delta \gtrless 90°$ for tensile earthquakes (volumetric source changes, see Appendix B). Let us note that for sources other than dislocation point sources, e.g. explosions or faulting on non-planar fault surfaces, inversions using Eq.(7) will yield $\nu_2 \neq 0$. Occurrence of $\nu_2 \neq 0$ may serve as an indication of an inadequate description of the seismic source by Eq.(3) or insufficient modelling of ray-path effects by $Y_{i\alpha}$. From a combination of the eigenvalues and the eigenvectors of $D_{pq}$ we get $s_i$, $n_i$, and $SA_0$ (see Appendix B). In fact, we obtain two vectors but we cannot uniquely identify from observations which is $s_i$ and which is $n_i$. We get two conjugate fault planes that are perpendicular to $s_i$ or $n_i$. These two planes are associated with the rupture plane and the auxiliary plane. They can make any angle. For shear faulting both planes are perpendicular. As in other source inversions, the rupture plane must be identified from additional information such as aftershock distribution or known fault-zone geometry. The

area of the fault $A_0$ and the length of the slip $S$ cannot be separated. From inversion we can only get the potency $SA_0$.

Given the retrieved source geometry, the moment tensor, which is usually sought in seismological practice, may be immediately computed from Eq.(3). The moment tensor can be decomposed into its double-couple (DC) and non-double-couple components, i.e. the compensated-linear-vector-dipole (CLVD) and the isotropic component (ISO). Several different decompositions of $M_{ij}$ have been proposed (see e.g. *Silver and Jordan, 1982*; *Jost and Herrmann, 1989*; *Vavryčuk, 2002*). Herein, we use equations of *Vavryčuk (2002)* that relate the moment-tensor components to the complete moment tensor. The (real or apparent) non-double-couple components have often been interpreted in terms of

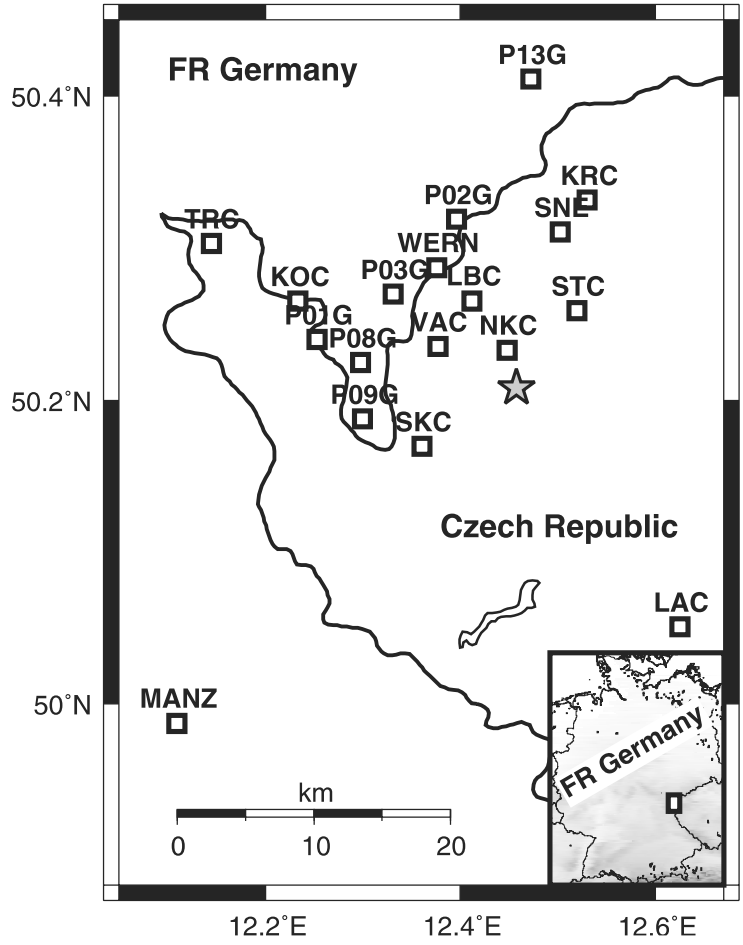


**Fig. 1.** Map of West Bohemia. Star: epicentre at 50.2085°N, 12.4576°E, 9.243 km depth, source time: October 15, 2000, 16:36:48. Squares: stations used for inversion of waveforms. See Table 1 for station parameters.

volumetric source changes connected to the faulting process. In anisotropic media, this interpretation might not be correct because the (apparent) non-double-couple moment-tensor components may be a consequence of neglected anisotropy (*Rössler et al., 2004*; *Vavryčuk, 2005*; *Rössler et al., 2007*). If, however, anisotropy is taken into account and the slip inclination $\delta$ differs from 90°, this is a more reliable indication of real volumetric source changes. The slip inclination is therefore considered as an important parameter during inversion. Possible conclusions made from the slip inclination and from the standard non-double-couple components may be later compared.

As a measure of strength of the event, we calculate the seismic moment $M_T$ from the moment tensor (*Silver and Jordan, 1982*):

$$M_T = \sqrt{\sum_{ij} M_{ij}^2 / 2} \,. \tag{11}$$

## 5. SOURCE RETRIEVAL FOR A $M_L$ = 3.1 EVENT FROM WEST BOHEMIA

### 5.1. Background and data

West Bohemia is a region of frequent earthquake swarm occurrence (see Fig. 1 for a map of the region). Studies of source mechanisms for the West Bohemia swarm episode in 1997 revealed volumetric components, which could be explained as indications for tensile faulting, i.e. shear faulting that is accompanied by volumetric source changes

**Table 1.** Parameters of stations used for source retrieval (see also Fig. 1). The sampling frequency of all stations is 250 Hz.

| Station | Lat [°N] | Lon. [°E] | Height [m] | Sensor | Institution |
|---|---|---|---|---|---|
| KOC | 50.26521 | 12.23352 | 575 | SM-3 | WEBNET |
| KRC | 50.33159 | 12.53028 | 760 | SM-3 | WEBNET |
| LAC | 50.05075 | 12.62495 | 838 | SM-3 | WEBNET |
| LBC | 50.26555 | 12.41218 | 638 | SM-3 | WEBNET |
| MANZ | 49.98710 | 12.10950 | 553 | STS-2 | U. Munich |
| NKC | 50.23312 | 12.44786 | 564 | SM-3 | WEBNET |
| P01G | 50.240 | 12.253 | 750 | LE-3D/5s | U. Potsdam |
| P02G | 50.319 | 12.396 | 630 | LE-3D/5s | U. Potsdam |
| P03G | 50.270 | 12.331 | 800 | LE-3D/5s | U. Potsdam |
| P08G | 50.225 | 12.298 | 710 | LE-3D/5s | U. Potsdam |
| P09G | 50.188 | 12.300 | 720 | LE-3D/5s | U. Potsdam |
| P13G | 50.411 | 12.472 | 480 | LE-3D/5s | U. Potsdam |
| SKC | 50.16980 | 12.36103 | 455 | LE-3D | WEBNET |
| SNE | 50.31072 | 12.50273 | 702 | SM-3 | WEBNET |
| STC | 50.25914 | 12.51965 | 666 | SM-3 | WEBNET |
| TRC | 50.30321 | 12.14452 | 566 | LE-3D | WEBNET |
| VAC | 50.23540 | 12.37710 | 535 | SM-3 | WEBNET |
| WERN | 50.2874 | 12.3761 | 630 | STS2 | U. Leipzig |

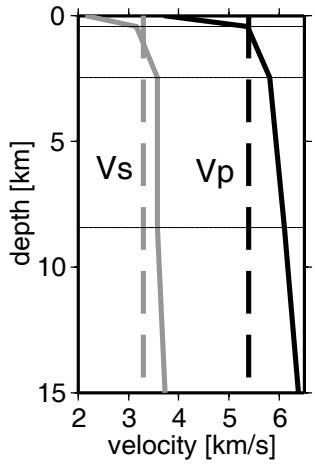


**Fig. 2.** P-wave (black) and S-wave (grey) velocities for West Bohemia (compare Table 2). Solid line: vertically inhomogeneous isotropic Model I (reference velocities for Model II) derived by *Málek et al., 2005*. Dashed line: homogeneous transversely isotropic Model III characterised by $v_p = \sqrt{\left(A_{11} + A_{22} + A_{33}\right)/3}$ , $v_s = \sqrt{\left(A_{44} + A_{55} + A_{66}\right)/3}$ (*Vavryčuk, 1993*).

during faulting. Existence of such volume changes follows from non-double-couple components of the retrieved moment tensors (*Vavryčuk, 2002*). Let us note that seismic anisotropy observed in this region (*Vavryčuk, 1993*; *Růžek et al., 2003*; *Málek et al., 2005*) was neither accounted for during interpretations nor during inversions for moment tensors. On the other hand, such non-double-couple components could not be explained by transversely isotropic media with up to 10% anisotropy (*Rössler et al., 2004*).

Several homogeneous and inhomogeneous isotropic velocity models were proposed for the focal area in West Bohemia (see e.g. *Novotný, 1996*; *Málek et al., 2004*). Three anisotropic/isotropic models used in this study and referred to as Models I-III, see Fig. 2 and Tables 2–4, were derived by *Málek et al. (2005)* and *Vavryčuk (1993)*.

**Model I** is a vertically inhomogeneous isotropic model derived by *Málek et al. (2005)*, see Fig. 2 and Table 2.

**Model II** is a vertically inhomogeneous, weak anisotropy model also derived by *Málek et al. (2005)*, see Fig. 2 and Table 3. The model has been derived from P waves only.

**Model III** is homogeneous and transversely isotropic. See Fig. 2 for averaged isotropic velocities and Table 4 for the elastic moduli. It has been derived from S-wave splitting and S-P travel time differences using effective medium theory (*Vavryčuk, 1993*).

We apply our inversion algorithm to one earthquake that occurred during the 2000 West Bohemia earthquake swarm episode. This earthquake swarm represents the most recent period of intense seismic activity in the region. It started on August 28, 2000 and lasted for 4 months. The events occurred on a fault, oriented in N-S direction at depths

**Table 2.** Model I. P- ( $v_p$ ) and S-wave ( $v_s$ ) velocities as function of depth (*Málek et al., 2005*). Cubic-spline interpolation is used. $v_s$ at 32 km depth is determined from $v_p/v_s = \sqrt{3}$, density $\rho = 2650$ kg m$^{-3}$.

| Depth [km] | 0.00 | 0.41 | 2.46 | 8.41 | 32.00 |
|---|---|---|---|---|---|
| $v_p$ [km s$^{-1}$] | 3.70 | 5.37 | 5.81 | 6.10 | 7.20 |
| $v_s$ [km s$^{-1}$] | 2.18 | 3.16 | 3.57 | 3.58 | 4.16 |

**Table 3.** Weak anisotropy (WA) parameters (see *Pšenčík and Gajewski, 1998*) that specify the Model II at all depths (*Málek et al., 2005*). The WA parameters and reference P-wave velocities taken from Model I are used to determine depth distribution of P-wave related stiffness parameters. Remaining parameters are determined from S-wave velocities of Model I.

| | $\varepsilon_x$ | $\varepsilon_y$ | $\varepsilon_z$ | $\delta_x$ | $\delta_y$ | $\delta_z$ | $\chi_x$ | $\chi_y$ | $\chi_z$ | $\varepsilon_{15}$ | $\varepsilon_{16}$ | $\varepsilon_{24}$ | $\varepsilon_{26}$ | $\varepsilon_{34}$ | $\varepsilon_{35}$ |
|---|---|---|---|---|---|---|---|---|---|---|---|---|---|---|---|
| $\times 10^{-3}$ | −12 | 7 | 11 | −4 | 6 | −5 | 9 | −4 | 1 | 2 | 7 | 3 | 7 | −7 | −5 |

**Table 4.** Model III. Density-normalised elastic parameters $A_{ij}$ in Voigt notation ( $A_{ij} = C_{ij}/\rho$ ) that describe a homogeneous anisotropic model for West Bohemia.

| | $A_{11}$ | $A_{12}$ | $A_{13}$ | $A_{22}$ | $A_{23}$ | $A_{33}$ | $A_{44}$ | $A_{55}$ | $A_{66}$ |
|---|---|---|---|---|---|---|---|---|---|
| $\times 10^6$ m$^2$s$^{-2}$ | 23.5 | 7.8 | 7.8 | 31.9 | 9.9 | 31.9 | 11.0 | 10.8 | 10.8 |

between 8 and 11 km. Accurate hypocentre locations are provided by *Bouškova (2005)*. The swarm has been subdivided into nine separate phases. The selected event represents the onset of the fifth phase. Hypocentre parameters are 50.2085°N, 12.4576°E, 9.243 km depth, source time is October 15, 2000, 16:36:48 (*T. Fischer, personal communication*). So far, a detailed study of source mechanisms of the year 2000 earthquake swarm has not yet been performed but indications of fluid related earthquake triggering have been found, e.g. by *Hainzl and Fischer (2002)*, *Fischer and Horálek (2005)*, *Hainzl and Ogata (2005)* and *Parotidis et al. (2005)*. Observations by *Hainzl and Ogata (2005)* indicate that changes in pore pressure by high-pressure crustal fluids may be important for the triggering of events at the beginning and also during the fifth phase of the swarm.

In addition to the permanent stations in the region, temporary stations were installed by the University of Potsdam, the WEBNET group, the Central Seismological Observatory and the GeoForschungsZentrum Potsdam at different periods during the swarm (see Table 1, Fig. 1, and *Klinge et al., 2003*). The selected event occurred at a time of maximum station coverage. Note that although many stations were available, ray coverage was non-uniform. For example, only one station in SE direction can be used for inversion.

### 5.2. Results of inversion

We invert three-component displacement seismograms of the P waves recorded at 18 stations (see Fig. 1 for their locations and Table 1 for their coordinates), for which the amplitude transfer functions are accurately known. We do not use S waves here because velocity Model II does not contain detailed information on S waves. Furthemore, most stations are situated at distances at which S waves are incident at the Earth's surface with an overcritical angle. Stations with unknown amplitude characteristics are not included. Seismograms are uniformly resampled to 0.01 s sampling interval. A time window of 0.4 s around the P wavelet is used for inversion. The similarity between the shape of observed and modelled waveforms is expressed by the cross-correlation coefficient. The cross-correlation coefficient for most traces is above 0.9. We exclude seismograms with complicated P wavelets that have cross-correlation coefficients below 0.6. Observed P waves are generally characterised by high signal-to-noise ratios and clear onsets (Fig. 3). The corner frequency of the studied event is around 10 Hz (Fig. 4). To reduce the effects of the source-time function of the events on the inversion, we low-pass filter data and synthetic seismograms at 10 Hz.

Using the Models I-III, similar fault-plane solutions are obtained (see Fig. 5 and Table 5) and the residuals are similarly reduced. Wavelets match well at all stations except the station LBC (Fig. 6, trace 9). The plane oriented in N-S direction is identified as the rupture plane. It can be associated with the map of the fault zone obtained from

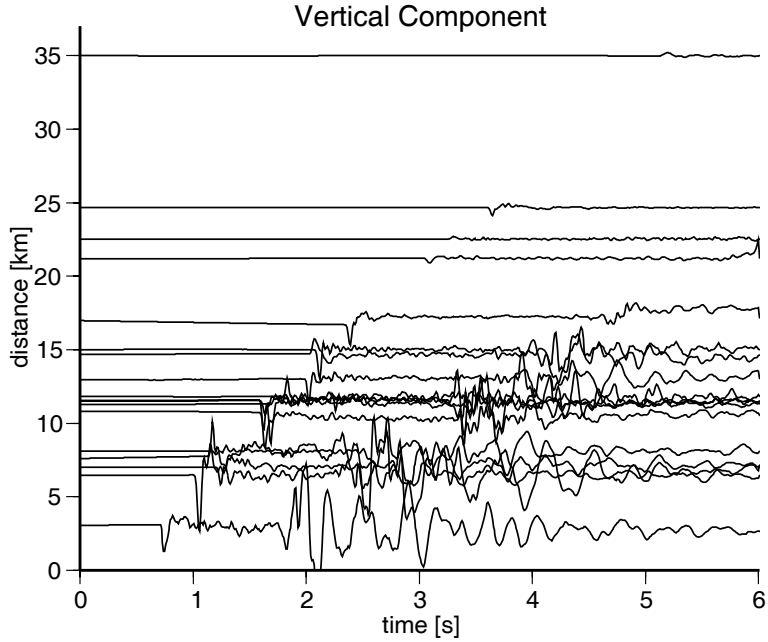


**Fig. 3.** Vertical-component seismograms (displacement) for stations and event shown in Fig. 1. Seismograms are unfiltered and sorted by epicentral distance. Positive amplitudes refer to upwards directed displacement. Source time corresponds to −1 s in the seismograms.

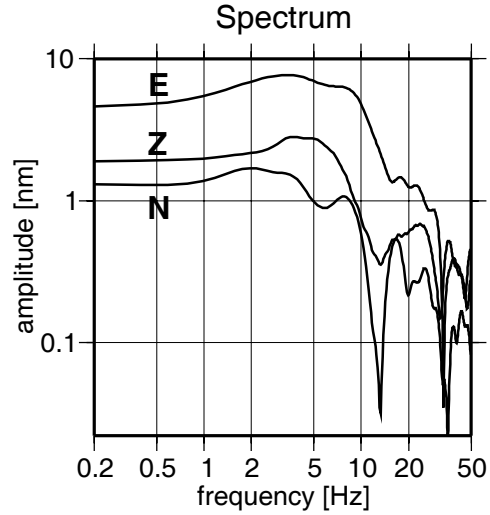


**Fig. 4.** Three-component displacement spectra of the P wave at NKC, the station closest to the epicentre.

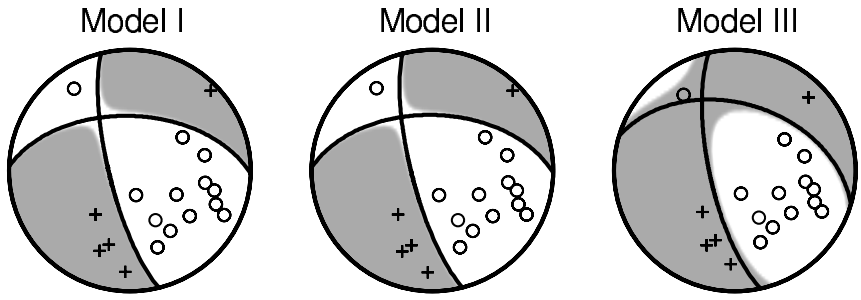


**Fig. 5.** Retrieved fault-plane solutions and P-wave radiation patterns for the velocity Models I, II, and III (lower-hemisphere projection). Grey areas indicate compression. Observed P-wave polarities are plotted in their take-off directions from the source to the stations in Fig. 1. Compressional and dilatational first motions are shown by crosses and circles, respectively.

located earthquake foci (*Fischer, 2003*). The event is therefore characterised by left-lateral oblique normal faulting on a N-S oriented fault plane dipping steeply towards the West. This orientation is similar to that obtained by *Fischer and Horálek (2005)* using the FOCMEC algorithm (*Snoke, 2003*). The retrieved dip-slip component is slightly larger for Model III as compared to the Models I and II. The seismic moment $M_T$, see Eq.(11), varies in the range $3.2 - 3.8 \times 10^{14}$ Nm. Using an empirical relation for local magnitudes $M_L$ in West Bohemia (*Hainzl and Fischer, 2002*) we find $M_L = 3.1$ for the event.

Retrieved sources comprise a small amount of tensile component (crack opening) indicated by $\delta < 90°$ for all three velocity models (see Table 5). The deviation from pure shear faulting (tensile character) is smallest for the inhomogeneous anisotropic Model II.

**Table 5.** Residual $R$, see Eq.(9), slip inclination $\delta$ as well as mean slip inclinations $\overline{\delta}$ and standard deviations $\sigma(\delta)$ obtained from bootstrap tests, orientation of the rupture plane, seismic moment $M_T$ ($M_T = M \times 10^{14}$ Nm), and moment-tensor components retrieved by using initial conditions and velocity Models I-III. (★) - inversion without station LBC.

| | | Slip Inclination [°] | | | Rupture Plane [°] | | | Moment Tensor [%] | | | |
|---|---|---|---|---|---|---|---|---|---|---|---|
| Model | $R$ | $\delta$ | $\overline{\delta}$ | $\sigma(\delta)$ | Strike | Dip | Rake | $M$ | DC | ISO | CLVD |
| I | 0.06 | 86.5 | 86.7 | 1.2 | 166 | 76 | –39 | 3.4 | 81.0 | +4.9 | +14.1 |
| I (★) | 0.06 | 87.6 | 87.8 | 1.1 | 168 | 75 | –42 | 3.5 | 90.0 | +7.8 | +2.2 |
| II | 0.06 | 86.8 | 86.9 | 1.2 | 166 | 76 | –40 | 3.6 | 82.0 | +4.9 | +13.1 |
| II (★) | 0.06 | 88.0 | 87.2 | 1.2 | 168 | 75 | –42 | 3.8 | 91.5 | +8.2 | –0.4 |
| III | 0.08 | 83.9 | 84.1 | 1.1 | 168 | 73 | –51 | 3.2 | 71.5 | +12.7 | +15.8 |
| III (★) | 0.08 | 84.3 | 84.4 | 1.3 | 169 | 73 | –52 | 3.3 | 74.8 | +17.1 | +8.2 |

For it, the slip vector deviates off the fault plane by 3.2° (Table 5). A small increase in the tensile character is observed for the inhomogeneous isotropic Model I. The non-double-couple components of the resulting moment tensors are also small and nearly equal for Models I and II (Table 5). The largest tensile components and largest non-double-couple moment-tensor components are retrieved for the homogeneous anisotropic Model III. For all velocity Models I-III, the eigenvalues of retrieved source tensor $D_{pq}$ in Eq.(5) are $\nu_1 \gg \nu_2$ and $\nu_3 \gg \nu_2$. This indicates that the determined source mechanisms are in accordance with the model for dislocation point sources assumed in Eqs.(3)–(5) and (10). The differences in solutions resulting from Models I/II and III can be explained by the structural differences causing differently modulated amplitudes in the modelled wavefield and different take-off directions of rays at the source (Fig. 7). Take-off directions are indistuingishable for rays in the Models I and II. Therefore, the small differences in source geometry for Models I and II most probably result from neglecting or accounting for anisotropy.

In our data example it seems that the retrieved source mechanism is more similar to a shear source when assuming more structural complexity including vertical inhomogeneity and P-wave anisotropy. Adding information on anisotropy from observations of S waves to the inhomogeneous anisotropic Model II could intensify this effect. However, accounting for structural inhomogeneity takes the largest effects on retrieved source parameters. Similar observations were made by *Ramos-Martínez and McMechan (2001)* using a finite-difference approach.

### 5.3. Jackknife and bootstrap tests

Only the inhomogeneous anisotropic Model II contains information on structural complexity and anisotropy. This model is therefore used to test the sensitivity of the inversion to variations of the station (receiver) distribution and of the weight of the data at a station by means of jackknife and bootstrap tests. These are nonparametric methods for assessing the errors in a statistical estimation problem, which apply to arbitrarily complicated situations without assumptions on distribution of uncertainties (*Efron, 1981*).

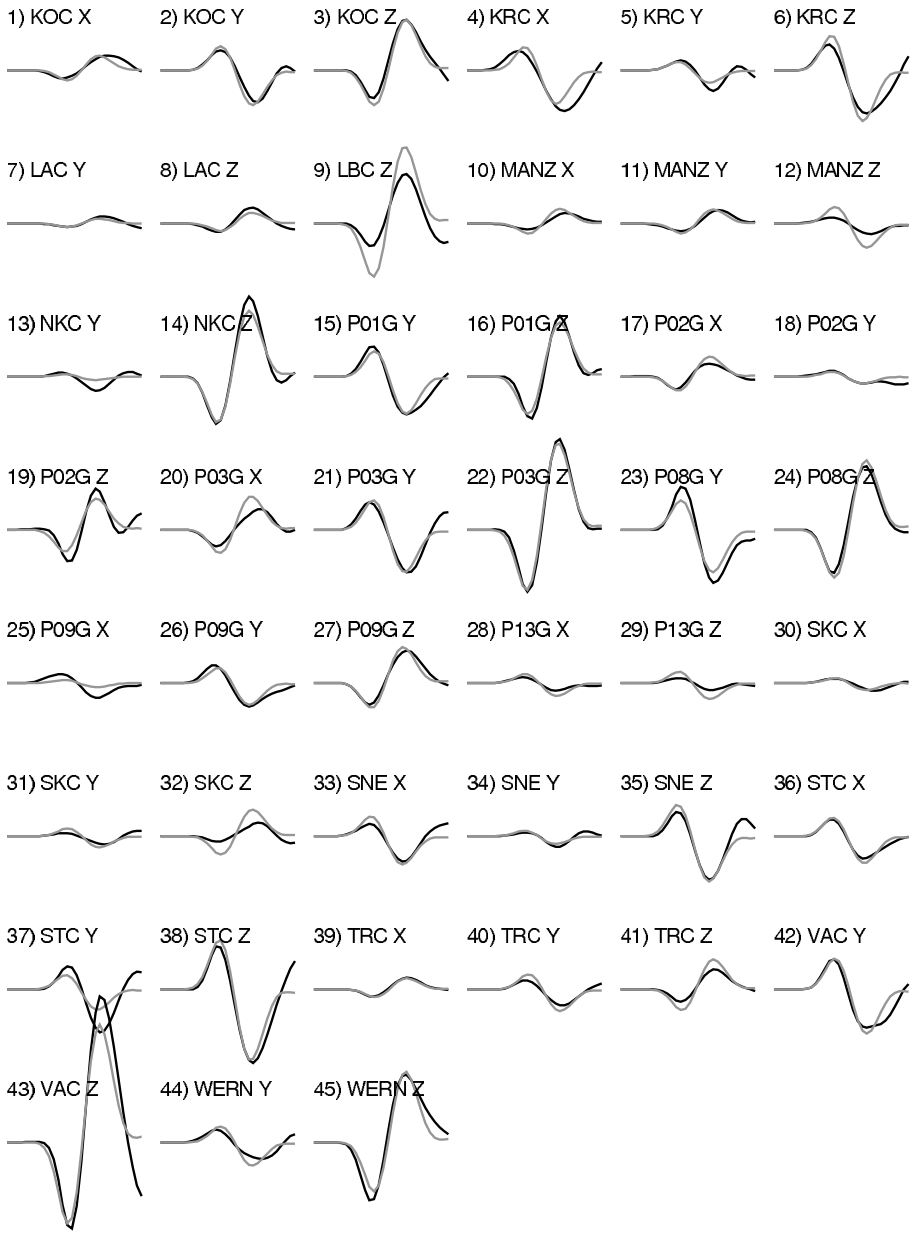


**Fig. 6.** 1–10 Hz band-pass filtered observed (black) and synthetic (grey) seismograms for stations used during inversion (see Fig. 1). Length of seismograms: 0.4 s, maximum amplitude: 6516 nm at VAC (trace 43). Trace number, station name and component are given above the seismograms. Notation of components: *X*-North, *Y*-East, *Z*-vertical, positive upwards. Components not shown here were excluded from inversion due to low correlation between data and synthetics.

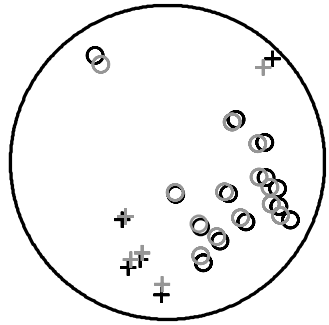

**Fig. 7.** Comparison of take-off directions of the P waves in Fig. 5 (lower-hemisphere projection) for the Models II (black), and III (grey). Take-off directions for P waves in Model I from Fig. 5 are not plotted. They are indistinguishable from take-off directions in Model II. First motion is compression (crosses) or dilatation (circles).

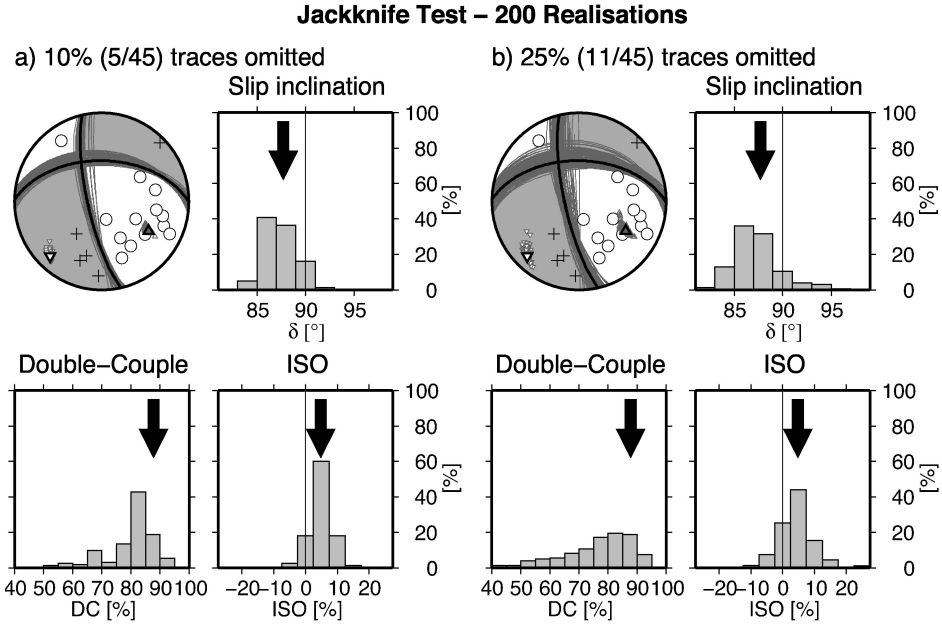


**Fig. 8.** Jackknife tests for event and stations shown in Fig. 1 using Model II. In 200 realisations, **a)** 10% and **b)** 25% of all available traces are randomly excluded from the inversions. Fault-plane solutions (grey curves) with *P* and *T* axes (grey triangles and grey inverted triangles, respectively) are plotted for each realisation as well as the distribution of corresponding slip inclinations ($\delta$) and moment-tensor components (DC, ISO). Fault-plane solutions and the *P* and *T* axes are plotted in black for unmodified conditions. The P-wave radiation pattern due to the retrieved source is underlying the fault-plane solutions: grey area - compression, white area - dilatation. Corresponding quantities are indicated by arrows in the histograms.

For jackknife testing, we randomly omit 10% or 25% of all traces available from all stations. The procedure is repeated 200 times (see Fig. 8 for results of the jackknife tests). We find that the fault orientation, slip inclination, and components of moment tensors are well constrained if the number of traces is randomly reduced by 10% (Fig. 8a). For most realisations the slip inclination varies between 85° and 89°. The retrieved double-couple and isotropic components are in the range of 75–90% and 0–10%, respectively. When reducing the number of traces by 25% (Fig. 8b), fault planes show a wider range of variability. Slip inclinations are in the same range as for the 10%-jackknife test. The distribution of double-couple and isotropic components is broadened and more moment tensors with small DC occur. For most realisations, isotropic components remain positive. The jackknife tests show that non-shear components are stable and tensile components are robust even if the ray coverage is varied. We can therefore rule out that the retrieved tensile source component is biased and an artefact of the non-uniform station distribution. Omitting more observations leads, however, to a reduction of this uniqueness.

During bootstrap tests we modify the weight of one single station during inversion by feeding the data of this station 1, 2, 5, 10, 20, 50 or 100 times into the system of equations (7), see Fig. 9. The procedure is repeated for every station while the weights of the remaining stations are kept constant and equal 1. For a station with a high weight factor the inversion aims to fit the amplitudes of this station preferentially. If rays to one

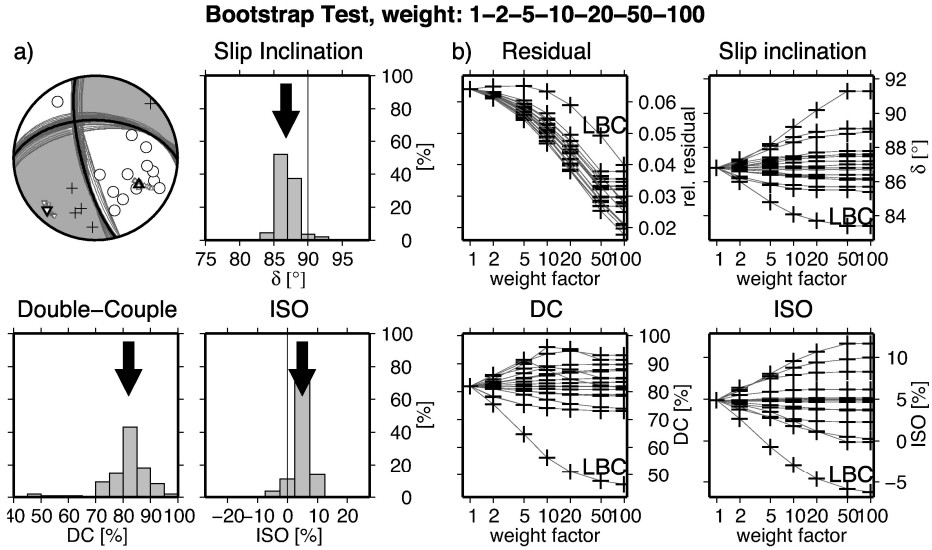


**Fig. 9.** Bootstrap tests for event and stations in Fig. 1 using the velocity Model II. During every realisation the weight of each station is varied (weight factors: 1, 2, 5, 10, 20, 50, 100) while the weight of remaining stations is one. The procedure is repeated for each station. **a)** Fault-plane solutions and source parameters retrieved by bootstrapping. See Fig. 8 for more details. **b)** Results for bootstrapping of individual stations (one curve - one station). Along every curve the weight of another station is varied while the weight of the remaining stations is kept constant and equal 1. Note outliers for bootstrapping of station LBC.

station are of special importance for the inversion, e.g. in case of an isolated station location, the solution can be stabilised by increasing the weight of this station. On the other hand, inversions may become unstable if amplitudes are inappropriately modelled at the station that is weighted higher. This can be the case for unknown heterogeneity along the particular raypath.

Retrieved fault-plane solutions show only minor variability for all bootstrap tests (Fig. 9a). Except for the station LBC the variations of the slip inclination, the moment-tensor components, and the residuals are close to each other (see Fig. 9b). The mean values of the slip inclinations are slightly larger than the values for the unchanged initial conditions (see Table 5). However, small standard deviations indicate that the tensile components are significant. Increasing weight for the station LBC causes deviation of all quantities. Observed DC < 70% in Fig. 9 is caused by overweighting the station LBC. Situated in a direction of dense ray coverage (compare Fig. 1) the influence of this station cannot be explained by its location. Therefore, the effect must be caused by the mismodelling of the P-wave amplitude (Fig. 6). Omitting the LBC station during the inversion leads to an increase in shear character ($\delta = 88°$ for otherwise unchanged initial conditions and Model II) and to an increase in the double-couple component of the moment tensor as well as to a slight rotation of the fault orientation (see Table 5). However, a small amount of non-shear component remains. A similar trend is also found for the Models I and III (see Table 5). Therefore, the observed tensile component does not seem to be an artefact of a mismodelled structure along a ray to a particular station.

The principial directions of the local stress field ($P$ and $T$ axes) are stable during testing (see Figs. 8 and 9). They indicate compression in SE–NW direction and tension in SW–NE which is similar to the stress field observed in West Bohemia and Central Europe before (*Wirth et al., 2000*; *Hinzen, 2003*; *Plenefisch and Klinge, 2003*).

### 5.4. Tests assuming different source depths

We have also carried out computations to evaluate the influence of mismodelled source depth. For the calculations of synthetic seismograms we considered all three velocity models and situated sources between 6 km and 14 km depth with a step of 500 m. Note that the depth uncertainty due to the localisation algorithm is about 100 m (*T. Fischer, personal communication*). Additional errors in source locations may occur due to ignored anisotropy in the localisation algorithm (*Málek et al., 2005*).

Residuals as well as retrieved slip inclinations and seismic moment tensors show sensitivity to source depth in all three Models I-III (Figs. 10–12). The fault orientation is rotated towards a larger strike slip component for shallower event depths.

Assuming the inhomogeneous isotropic Model I, a minimum residual is reached at 2 km above the localisation depth (Fig. 10). In this case, the slip inclination $\delta$ indicates almost pure shear faulting. A maximum of the DC moment-tensor component is reached for a source depth below 8 km. The seismic moment and the size of the isotropic moment-tensor component increase whereas the slip inclination decreases monotonously with the assumed source depth.

Similar observations are made for the inhomogeneous anisotropic Model II. In contrast to Model I, the smallest residuals are observed for source depths between 8 and 9 km, thus closer to the localisation depth, which is 9.24 km. Retrieved seismic moments are slightly

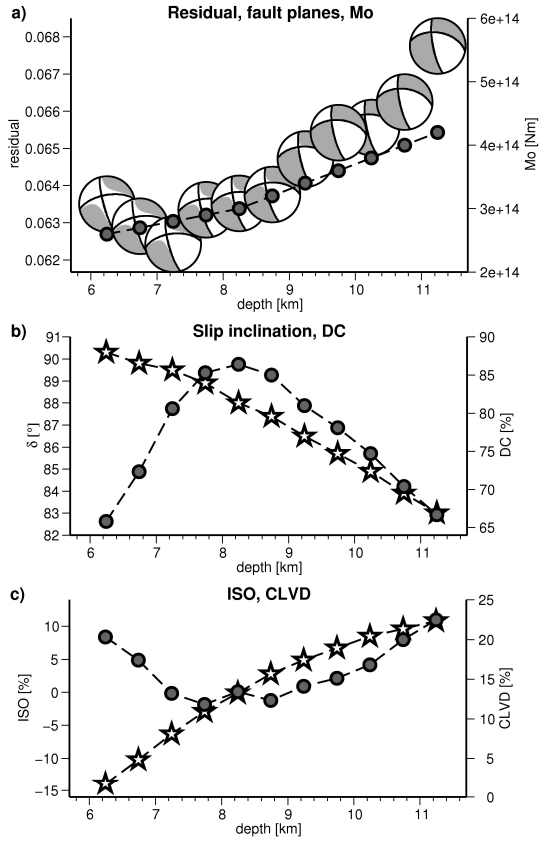


**Fig. 10.** Source parameters vs. source depth obtained from inversions assuming velocity Model I. Epicentre position and stations are shown in Fig. 1. Localised source depth: 9.243 km. **a)** Fault-plane solutions positioned at residual values $R$ and seismic moments $M_T$ (circles). **b)** Slip inclinations $\delta$ (stars) and DC moment-tensor components (circles). **c)** non-DC moment-tensor components: ISO (stars) and CLVD (circles).

increased. In contrast to Model I, the minimum of the residual function and the CLVD coincide with the maximum of the DC. This can be understood as an effect of considering anisotropy.

For the homogeneous anisotropic Model III, the residual function shows a broader minimum at 11–13 km source depth, thus significantly below the localised source depth. Seismic moments are slightly larger than for the Models I and II. No extremum is observed for the deviatoric moment-tensor components in the considered depth range. The fault plane solutions contain an increased dip-slip component. The different behaviour of the residual function and the source orientation as compared to the Models I and II can be partly explained by increased angles of incident waves at the surface. Models I and II contain a near-surface low-velocity zone that is missing in Model III. Therefore, angles of

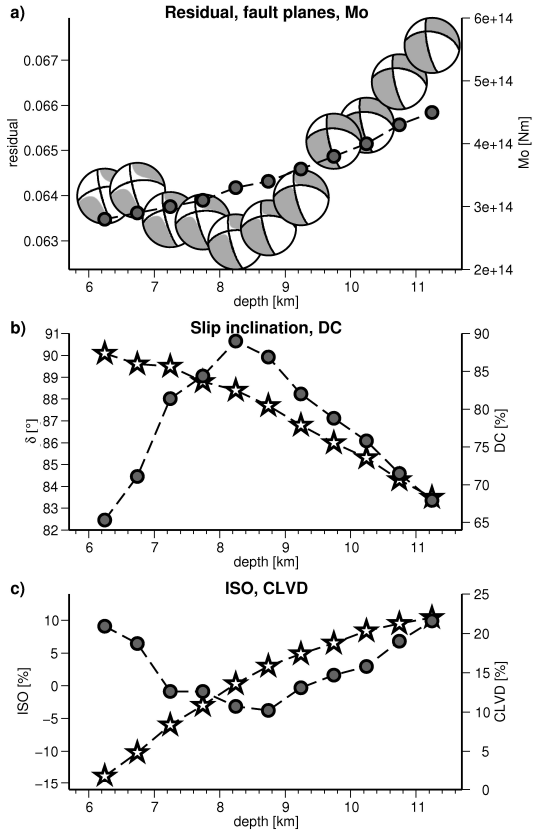


**Fig. 11.** As in Fig. 10 but for velocity Model II.

incident waves are steeper in Models I and II than in Model III. Consequently, for sources in Model III, greater hypocentre depths are required to obtain the same incidence angles at the surface. This explains why the smallest residuals in Model III can be found at greater depth than in Models I and II. As a result, different take-off angles in Models I/II and III lead to a rotation of the retrieved source mechanisms.

## 6. CONCLUSIONS

We have introduced an algorithm to retrieve the geometry of dislocation point sources in anisotropic media from observed waveforms. Decoupling the source geometry from the elastic properties of the medium surrounding the source allows direct interpretation of the retrieved source mechanism in terms of possible volumetric source changes. Hereby, reasonable knowledge of anisotropy in the focal area is required. The geometry and the size of the source are characterised by the normal to the fault plane, the direction of the

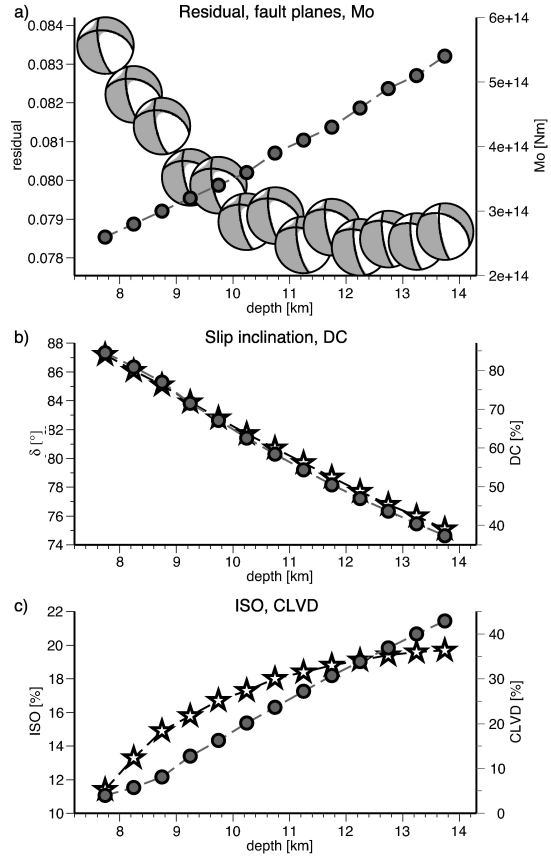


**Fig. 12.** As in Fig. 10 but for velocity Model III.

slip, the fault area, and the size of the slip. Fault normal and slip vector may be arbitrarily oriented. Thus, shear faulting as well as tensile faulting are allowed. Deviations from the dislocation model may be found by an eigenvalue analysis of the source tensor $D_{pq}$. The inversion scheme is based on fitting synthetic seismograms to observed ones. For computation of synthetic seismograms we apply ray methods for isotropic or anisotropic media, which represent a basis of the ANRAY software package (*Pšenčík, 1998*). The algorithm is therefore time-effective and applicable in standard data processing. The success of the proposed inversion scheme depends on the accuracy of the used structural model.

The inversion algorithm was applied to a selected event of the earthquake swarm that occurred in West Bohemia in 2000. We observe $M_T \approx 3.4 \times 10^{14}$ Nm and left-lateral strike oblique normal faulting. The source mechanism retrieved for this event is in agreement with the model for dislocation point sources. A small amount of crack opening is indicated. Although it is only slight, this feature seems to be generally stable and

significant for different structural models, different assumptions about source depth and for changing station coverage. The *P* and *T* axes obtained from the retrieved source mechanisms are in agreement with other independent observations of the stress conditions in West Bohemia and Central Europe. The event occurred during the swarm phase five for which fluid-controlled event triggering has been proposed by *Hainzl and Ogata (2005)*. Our observation of tensile components coincides with this finding and seems to support it.

The results of inversion are constrained by jackknife and bootstrap tests as well as tests assuming different velocity models and uncertainties in source depth in these velocity models. In this way, inappropriate interpretation caused by errors due to mismodelling of the velocity structure is avoided. Accounting for structural 1D inhomogeneity has a significant effect on the solution. Taking into account anisotropy in the inhomogeneous Model II leads to a slight decrease in the tensile component of the obtained source mechanism. In Model II, anisotropy is derived from information of P waves only. Changes in anisotropy caused by considering S waves are expected to further affect the results. Effects due to more complicated source-time functions are diminished by excluding frequencies above the corner frequency of the event. The influence of intrinsic attenuation, near-source inhomogeneity, e.g., crack induced changes in near-source anisotropy, and source finiteness are not considered here.

We have recently applied the algorithm also to a larger amount of events in West Bohemia that occurred in 2000. There, we found spatial and temporal variations of tensile components.This will be presented in a follow-up publication. So far, recent results can be obtained from the website: *http://www.geo.uni-potsdam.de/forschung/geophysik/mominv/mominv.htm*.

Future applications of the introduced inversion algorithm can be seen where accurate determination of source mechanisms is of superior interest and where well-defined anisotropic velocity models exist, e.g. in a vicinity of a borehole or in carbonhydrate production fields.

*Acknowledgements:* This contribution was presented at the workshop "Seismic waves in laterally inhomogeneous media VI", Hrubá Skála, Czech Republic, June 20–25, 2005. Support of the German Science Foundation (DFG, grants KR1935/1-1 and KR1935/1-3), of the Charles University, Prague, through the MAGMA project, of the Geophysical Institute, Acad. Sci. Czech Republic, grant A300120502 of the Grant Agency of the Czech Republic, and of the consortium project SW3D is appreciated. The following people are acknowledged for data provision: T. Fischer (Geophysical Institute, Acad. Sci. Czech Republic), Th. Plenefisch (SZGRF), S. Funke (University of Leipzig), J. Wassermann (University of Munich) as well as colleagues and students from the University of Potsdam. We thank two anonymous reviewers for their comments that helped to improve the manuscript.

# APPENDIX A
# EQUATIONS FOR SOURCE RETRIEVAL

Equations (7) are derived from Eqs.(1)–(3) and (6) in the following way:

$$u_i(\boldsymbol{x},t) = g_i(\boldsymbol{x})\left[\frac{\rho(\boldsymbol{x}_0)c(\boldsymbol{x}_0)}{\rho(\boldsymbol{x})c(\boldsymbol{x})}\right]^{1/2} \frac{D\,f^{(A)}\left(t-\tau(\boldsymbol{x})\right)}{\left|\Omega_M(\boldsymbol{x})\right|^{1/2}} \exp\left[\mathrm{i}\frac{\pi}{2}k_s - \mathrm{i}\frac{\pi}{2}k(\boldsymbol{x}_0,\boldsymbol{x})\right] \tag{A.1}$$
$$= A_i B_{jk} s_p n_q c_{pqjk} S A_0 f^{(A)}\left(t-\tau(\boldsymbol{x})\right)\exp\left[\mathrm{i}\frac{\pi}{2}k_s - \mathrm{i}\frac{\pi}{2}k(\boldsymbol{x}_0,\boldsymbol{x})\right].$$

In Eq.(A.1) we use the following notations:

$$A_i = \frac{g_i(\boldsymbol{x})}{\left(\rho(\boldsymbol{x})c(\boldsymbol{x})\right)^{1/2}} \frac{1}{\left|\Omega_M(\boldsymbol{x})\right|}, \tag{A.2}$$

$$B_{jk} = \frac{g_j(\boldsymbol{x}_0)p_k(\boldsymbol{x}_0)}{4\pi\left(\rho(\boldsymbol{x}_0)c(\boldsymbol{x}_0)\right)^{1/2}}. \tag{A.3}$$

From Eq.(A.1), we obtain Eq.(A.4), which is Eq.(7)

$$\mathrm{Re}\left(u_i(\boldsymbol{x},t)\right) = Y_{i\alpha}\,\mathrm{Re}\left(f^{(A)}\left(t-\tau(\boldsymbol{x})\right)\exp\left[\mathrm{i}\frac{\pi}{2}k_s - \mathrm{i}\frac{\pi}{2}k(\boldsymbol{x}_0,\boldsymbol{x})\right]\right)\sigma_\alpha. \tag{A.4}$$

The fourth-order elastic tensor $c_{ijkl}$ can be written in the Voigt notation $C_{\alpha\beta}$ (attributed to *Voigt, 1928*) by contracting pairs of indices $i, j$ to a single index $\alpha$ ($ij \leftrightarrow \alpha$). Applying the relations $11 \leftrightarrow 1$, $22 \leftrightarrow 2$, $33 \leftrightarrow 3$, $23 \leftrightarrow 4$, $13 \leftrightarrow 5$, $12 \leftrightarrow 6$ (*Musgrave, 1970*), the quantities $Y_{i\alpha}$ in Eq.(7) are obtained

$$Y_{i\alpha} = X_{i\beta}C_{\alpha\beta}, \tag{A.5}$$

where

$$\begin{aligned} X_{i1} &= A_i B_{11}, \\ X_{i2} &= A_i B_{22}, \\ X_{i3} &= A_i B_{33}, \\ X_{i4} &= A_i\left(B_{23}+B_{32}\right), \\ X_{i5} &= A_i\left(B_{13}+B_{31}\right), \\ X_{i6} &= A_i\left(B_{12}+B_{21}\right). \end{aligned} \tag{A.6}$$

## APPENDIX B
## SLIP AND FAULT NORMAL FROM THE SOURCE TENSOR

The orientation of the slip $s_i$, the fault normal $n_i$, and the product of fault area $A_0$ and the length of the slip $S$ (the potency) are determined from the eigenvalues $\nu_i$ and the corresponding eigenvectors $\boldsymbol{e}_i$ of the source tensor $D_{ij}$. The eigenvalues of $D_{ij}$ read (compare *Vavryčuk, 2005*)

$$\nu_1 = \frac{SA_0}{2}\left(s_i n_i + 1\right), \quad \nu_2 = 0, \quad \nu_3 = \frac{SA_0}{2}\left(s_i n_i - 1\right). \tag{B.1}$$

They can be also written as

$$\nu_1 = \frac{SA_0}{4}\left(\boldsymbol{s}+\boldsymbol{n}\right)\cdot\left(\boldsymbol{s}+\boldsymbol{n}\right), \quad \nu_2 = 0, \quad \nu_3 = \frac{SA_0}{4}\left(\boldsymbol{s}-\boldsymbol{n}\right)\cdot\left(\boldsymbol{s}-\boldsymbol{n}\right). \tag{B.2}$$

The corresponding (normalised) eigenvectors are

$$\boldsymbol{e}_1 = \frac{\boldsymbol{s}+\boldsymbol{n}}{\left|\boldsymbol{s}+\boldsymbol{n}\right|}, \quad \boldsymbol{e}_2 = \frac{\boldsymbol{s}\times\boldsymbol{n}}{\left|\boldsymbol{s}\times\boldsymbol{n}\right|}, \quad \boldsymbol{e}_3 = \frac{\boldsymbol{s}-\boldsymbol{n}}{\left|\boldsymbol{s}-\boldsymbol{n}\right|}, \tag{B.3}$$

where $\times$ denotes the vectorial product. Then, $s_i$, $n_i$, and $SA_0$ are determined from Eqs.(B.2) and (B.3)

$$\boldsymbol{s} = \frac{\boldsymbol{e}_1\sqrt{\nu_1}+\boldsymbol{e}_3\sqrt{\nu_3}}{\left|\boldsymbol{e}_1\sqrt{\nu_1}+\boldsymbol{e}_3\sqrt{\nu_3}\right|}, \quad \boldsymbol{n} = \frac{\boldsymbol{e}_1\sqrt{\nu_1}-\boldsymbol{e}_3\sqrt{\nu_3}}{\left|\boldsymbol{e}_1\sqrt{\nu_1}-\boldsymbol{e}_3\sqrt{\nu_3}\right|}, \quad SA_0 = \nu_1 - \nu_3. \tag{B.4}$$

*References*


Aki K. and Richards P.G, 2002. *Quantitative Seismology*. University Science Books, Sausalito, CA, USA.

Boušková A., 2005. *Catalogue of Seismic Events*. Geophysical Institute, Academy of Sciences of the Czech Republic, Prague. Online at http://www.ig.cas.cz/seismo/Webnet/.

Červený V., 2001. *Seismic Ray Theory*. Cambridge University Press, Cambridge, U.K.

Dahm T., Horálek J. and Šílený J., 2000. Comparison of absolute and relative moment tensor solutions for the January 1997 West Bohemia earthquake swarm. *Stud. Geophys. Geod.*, **44**, 233–250.

Dreger S.D., Tkalčič H. and Johnston M., 2000. Dilational processes accompanying earthquakes in the Long Valley Caldera. *Science*, **288**, 122–125.

Efron B., 1981. The nonparametric estimates of standard errors - the jackknife, the bootstrap and other methods. *Biometrika*, **68**, 589–599.

Fischer T., 2003. The August–December 2000 earthquake swarm in NW Bohemia: the first results based on automatic processing of seismograms. *J. Geodynamics*, **35**, 59–81.

Fischer T. and Horálek J., 2005. Slip-generated patterns of swarm microearthquakes from West Bohemia/Vogtland (Central Europe): Evidence of their triggering mechanism? *J. Geophys. Res.*, **110**, B05S21, doi:10.1029/2004JB003363.

Foulger G.R., Julian B.R., Hill D.P., Pitt A.M., Malin P.E. and Shalev E., 2004. Non-double-couple microearthquakes at Long Valley caldera, California, provide evidence for hydraulic fracturing . *J. Volcanol. Geotherm. Res.*, **132**, 45–71.

Gajewski D., 1993. Radiation from a point source in general anisotropic media. *Geophys. J. Int.*, **113**, 299–317.

Hainzl S. and Fischer T., 2002. Indications for a successively triggered rupture growth underlying the 2000 earthquake swarm in Vogtland/NW Bohemia. *J. Geophys. Res.*, **107**, 2338, doi:10.1029/2002JB001865.

Hainzl S. and Ogata Y., 2005. Detecting fluid signals in seismicity data through statistical earthquake modelling. *J. Geophys. Res.*, **110**, B05S07, doi:10.1029/2004JB003247.

Henry C., Woodhouse J.H. and Das S., 2002. Stability of earthquake moment tensor inversions: effect of the double-couple constraint. *Tectonophysics*, **356**, 115–124.

Hinzen K.G., 2003. Stress field in the Northern Rhine area, Central Europe, from earthquake fault plane solutions. *Tectonophysics*, **377**, 325–356.

Jost M.L. and Herrmann R.B., 1989. A student's guide to and review of moment tensors. *Seism. Res. Letters*, **60**, 37–57.

Julian B.R., Miller A.D. and Foulger G.R., 1997. Non-double-couple earthquake mechanisms at the Hengill-Grensdalur volcanic complex, Southwest Iceland. *Geophys. Res. Lett.*, **24**, 743–746.

Julian B.R., Miller A.D. and Foulger G.R., 1998. Non-double-couple earthquakes, 1. theory. *Rev. Geophys.*, **36**, 525–549.

Kanamori H., Ekström G., Dziewonski A., Barker J.S. and Sipkin S.A., 1993. Seismic radiation by magma injection: An anomalous seismic event near Tori Shima, Japan. *J. Geophys. Res.*, **98**, 6511–6522.

Kawasaki I. and Tanimoto T., 1981. Radiation patterns of body waves due to the seismic dislocation occuring in an anisotropic source medium. *Bull. Seismol. Soc. Amer.*, **71**, 37–50.

Klinge K., Plenefisch T. and Stammler K., 2003. The earthquake swarm 2000 in the region Vogtland/NW-Bohemia - earthquake recording at German stations and temporal distribution of events. *J. Geodynamics*, **35**, 83–96.

Kuge K., 1994. Data-dependent non-double-couple-components of shallow earthquake source mechanisms: Effects of waveform inversion stability. *Geophys. Res. Lett.*, **21**, 9–12.

Málek J., Janský J., Novotný O., Rössler D. and the CELEBRATION 2000 Working Group, 2004. Vertically inhomogeneous models of the upper crustal structure in the West-Bohemian seismoactive region inferred from the CELEBRATION 2000 refraction data. *Stud. Geophys. Geod.*, **48**, 709–730.

Málek J., Horálek J. and Janský J., 2005. One-dimensional qP-wave velocity model of the upper crust for the West Bohemia/Vogtland earthquake swarm region. *Stud. Geophys. Geod.*, **49**, 709–730.

Menke W., 1989. *Geophysical Data Analysis: Discrete Inverse Theory. International Geophysics Series*, **Vol.45**. Academic Press, San Diego, USA.

Miller A.D., Foulger G.R. and Julian B.R., 1998. Non-double-couple earthquakes, 1. observations. *Rev. Geophys.*, **36**, 551–568.

Musgrave M.J.P., 1970. *Crystal Acoustics.* Holden-Day, San Fransisco, USA.

Novotný O., 1996. A preliminary seismic model for the region of the West-Bohemian earthquake swarms. *Stud. Geophys. Geod.*, **40**, 353–366.

Parotidis M., Shapiro S.A. and Rothert E., 2005. Evidence for triggering of the Vogtland swarms 2000 by pore pressure diffusion. *J. Geophys. Res.*, **110**, B05S10, doi:10.1029/2004JB003267.

Plenefisch T. and Klinge K., 2003. Temporal variations of focal mechanisms in the Nový Kostel focal zone (Vogtland/NW-Bohemia) - comparison of the swarms 1994, 1997 and 2000. *J. Geodynamics*, **35**, 145–156.

Pšenčík I., 1998. *ANRAY Package, Version 4.10*. Dept. of Geophysics, Charles University, Prague, Czech Republic, 403–404. Online at http://sw3d.mff.cuni.cz.

Pšenčík I. and Gajewski D., 1998. Polarization, phase velocity, and NMO velocity of qP-waves in arbitrary weakly anisotropic media. *Geophysics*, **63**, 1754–1766.

Pšenčík I. and Teles T.N., 1996. Point source radiation in inhomogeneous anisotropic structures. *Pure Appl. Geophys.*, **148**, 591–623.

Ramos-Martínez J. and McMechan G.A., 2001. Source-parameter estimation by full waveform inversion in 3D heterogeneous, viscoelastic, anisotropic media. *Bull. Seismol. Soc. Amer.*, **91**, 276–291.

Rössler D., Rümpker G. and Krüger F., 2004. Ambiguous moment tensors and radiation patterns in anisotropic media with applications to the modeling of earthquake mechanisms in W-Bohemia. *Stud. Geophys. Geod.*, **48**, 233–250.

Rössler D., Pšenčík I., Krüger F. and Rümpker G., 2005. Retrieval of source parameters for local earthquakes in anisotropic media. Dept. of Geophysics, Charles University, Prague, Czech Republic, 333–344. Online at http://sw3d.mff.cuni.cz.

Rössler D., Krüger F. and Rümpker G., 2007. Inversion for seismic moment tensors in anisotropic media using standard techniques for isotropic media. *Geophys. J. Int.*, **169**, 136–148, doi:10.1111/j.1365-246X.2006.03243.x.

Růžek B., Vavryčuk V., Hrubcová P., Zedník J. and the CELEBRATION Working Group, 2003. Crustal anisotropy in the Bohemian Massif, Czech Republic: observations based on Central European lithospheric experiment based on refraction CELEBRATION 2000. *J. Geophys. Res.*, **108**, 2392, doi:10.1029/2002JB002242.

Silver G.P. and Jordan T.H., 1982. Optimal estimation of the scalar seismic moment. *Geophys. J. R. Astr. Soc.*, **70**, 755–787.

Sipkin S.A., 1986a. Estimation of earthquake source parameters by the inversion of waveform data: global seismicity, 1981–1983. *Bull. Seismol. Soc. Amer.*, **76**, 1515–1541.

Sipkin S.A., 1986b. Interpretation of non-double-couple earthquake mechanisms derived from moment tensor inversions. *J. Geophys. Res.*, **91**, 531–547.

Snoke J.A., 2003. FOCMEC: FOcal MEChanism determinations. In: W. Lee, H. Kanamori, P. Jennings and C. Kisslinger (Eds.), *International Handbook of Earthquake and Engineering Seismology*. Academic Press, San Diego USA, Part B, 1629–1630 (and accompanying CD).

Solomon S.C. and Julian B.R., 1974. Seismic constraints on ocean-ridge mantle structure: anomalous fault plane solutions from first motions. *Geophys. J. R. Astr. Soc.*, **38**, 265–285.

Sykes L.R., 1967. Mechanism of earthquakes and nature of faulting on the mid-ocean ridges. *J. Geophys. Res.*, **72**, 5–27.

Vavryčuk V., 1993. Crustal anisotropy from local observations of shear-wave splitting in West Bohemia, Czech Republic. *Bull. Seismol. Soc. Amer.*, **83**, 1420–1441.

Vavryčuk V., 2001. Inversion for parameters of tensile earthquakes. *J. Geophys. Res.*, **106**, 16339–16355.

Vavryčuk V., 2002. Non-double-couple earthquakes of 1997 January in West Bohemia, Czech Republic: evidence of tensile faulting. *Geophys. J. Int.*, **149**, 364–373.

Vavryčuk V., 2005. Focal mechanisms in anisotropic media. *Geophys. J. Int.*, **161**, 334–346.

Voigt W., 1928. *Lehrbuch der Kristallphysik.* Teubner-Verlag, Leipzig, Germany.

Wirth W., Plenefisch T., Klinge K., Stammler K. and Seidl D., 2000. Focal mechanisms and stress field in the region Vogtland/Western Bohemia. *Stud. Geophys. Geod.*, **44**, 126–141.